Morphological and optical characteristics of nanocrystalline TiO_2 thin films by quantitative optical anisotropy and imaging techniques

2006 Meas. Sci. Technol. 17 436

(http://iopscience.iop.org/0957-0233/17/2/027)

INSTITUTE OF PHYSICS PUBLISHING MEASUREMENT SCIENCE AND TECHNOLOGY

Meas. Sci. Technol. **17** (2006) 436–440 doi:10.1088/0957-0233/17/2/027

Morphological and optical characteristics of nanocrystalline TiO_2 thin films by quantitative optical anisotropy and imaging techniques

Cong Ye[1], Sean Liu[2], Xuemei Teng[1], Qi Fang[1,3] and Guanghai Li[1]

[1] Key Laboratory of Materials Physics, Institute of Solid State Physics, Chinese Academy of Sciences, Hefei 230031, People's Republic of China
[2] Oxford Cryosystems Ltd, Long Hanborough, Oxford OX29 8LN, UK
[3] Department of Electronic and Electrical Engineering, University College London, London WC1E 7JE, UK

E-mail: ghli@issp.ac.cn

Received 14 September 2005, in final form 1 December 2005
Published 19 January 2006
Online at stacks.iop.org/MST/17/436

Abstract

TiO_2 thin films were prepared by dc reactive sputtering with different ratios of oxygen to argon. The optical characteristics of the films were studied by birefringence imaging and optical anisotropic analysis using MetriPol. A clear trend of aggregation and structural variation of TiO_2 nanoparticles in the films can be seen using MetriPol optical anisotropic imaging. It was found that the optical characteristics of the TiO_2 thin films depend on the ratios of O_2/Ar during sputtering of the films. The optical anisotropies are closely related to the structural feature of TiO_2 nanoparticles. Variation trends of TiO_2 film structures and optical characters have also been confirmed by FESEM observations and refractive index.

Keywords: DC reactive sputtering, titania, birefringent imaging, optical characteristics

(Some figures in this article are in colour only in the electronic version)

1. Introduction

TiO_2 as a transitional metal oxide has raised substantial interest in both industrial applications and scientific research in the last few years [1–6]. Due to their unique dielectric and optical properties, TiO_2 films are excellent in antireflection coating, optical interference filtering and optical wave guides [7–10]. Different processing techniques such as sol–gel processes [11], chemical vapour deposition [12], ion-assisted deposition [13], sputtering [14–16] and pulsed laser deposition [17] have been used to fabricate TiO_2 thin films. Among these techniques, reactive sputtering is easy in process and quality control so it is well industrially adopted.

To determine the relationship between the TiO_2 phase structure and film morphology and its stoichiometric conditions to gain a better understanding of optical properties, a number of imaging and data analysis techniques have been newly developed by using optical polarization states in reflection and transmission. In this paper, the so-called rotating-polarizer method, MetriPol, has been demonstrated (see www.metripol.com). This method creates false-colour images representing the non-perturbed light transmission I_0, the extinction angle ϕ (orientation of the vibration direction of the slow axis) and the modulated sine of phase retardation caused by birefringence, $|\sin\delta|$, which in many cases is a measurement of optical anisotropy. It also provides a lot of data useful for a quantitative phase structure, particle compactness and aggregation analysis. This technique has been successfully used to determine the morphotropic phase boundary and phase transition [18, 19].

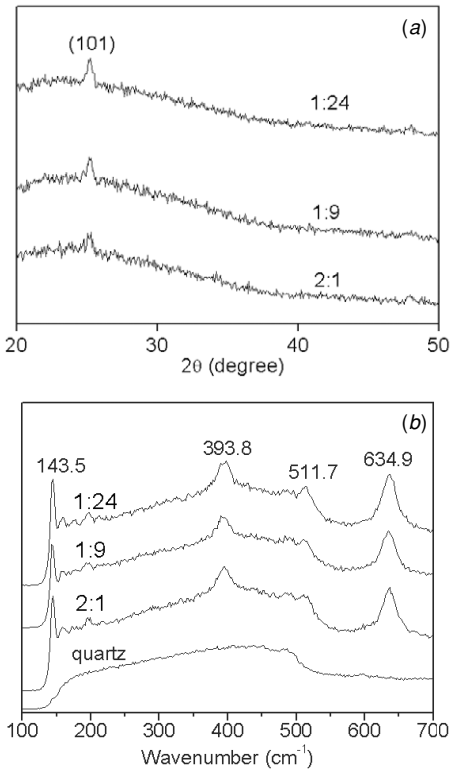

Figure 1. The XRD patterns (*a*) and Raman spectra (*b*) of the TiO_2 thin films with different O_2/Ar ratios.

2. Experimental details

TiO_2 thin films were grown by dc reactive sputtering using pure metallic titanium (99.999%) as the sputtering target. Single-side-polished silicon wafers with (1 0 0) orientation and quartz were used as the substrate. Pure oxygen (99.999%) and argon (99.999%) were respectively used as reactive and sputtering gases. The base pressure of the vacuum chamber is about 7×10^{-5} Pa. Sputtering was carried out at a pressure of 5.8 Pa in three O_2/Ar ratios (1:24, 1:9 and 2:1) and the total flow rate of the two gases which were controlled by mass flow controller was fixed at 30 $cm^3\,min^{-1}$. DC input power was approximately 120 W. The substrate temperature was maintained at 623 K. The distance between the target and the substrate was kept at 64 mm. Before each deposition, the target was pre-sputtered in Ar atmosphere for 20 min to remove surface oxides on the target surface. In this paper, we assigned respectively the films sputtered with O_2/Ar ratios of 1:24, 1:9 and 2:1 (2.8%, 7.2% and 58% oxygen) as samples A, B and C for convenience.

Grazing angle x-ray diffraction (XRD, INCA Energy X-ray microanalysis system with Cu κ_α radiation), Raman spectra (Nexus spectrometer) and field-emission scanning electron microscopy (FESEM, Sirion 200, resolution, 2.0 nm at 1 kV) were used to study the phase structures and morphologies of the films. The optical constants were obtained by a Jobin-Yvon ellipsometer over the spectral range of 200−1600 nm. The angle of incidence is 70° with 1 mm diameter spot size.

Birefringence imaging analyses were made using the MetriPol Addon version in a Leica microscope at room temperature. Both linear birefringence and orientation data and colour-coded images have been collected and analysed. During the measurement, white light was filtered into single colour and incident with dynamically variable polarization angles into the sample and the transmission altered by the sample's polarization states has been collected with a digital camera. The collected pixellized data are then modelled and solved to derive the birefringence ($|\sin\delta|$), orientation (ϕ) and transmission (I_0) values and finally presented as colour-coded images. These data bearing the information of microscopic optical anisotropy can be exported and plotted in line and area

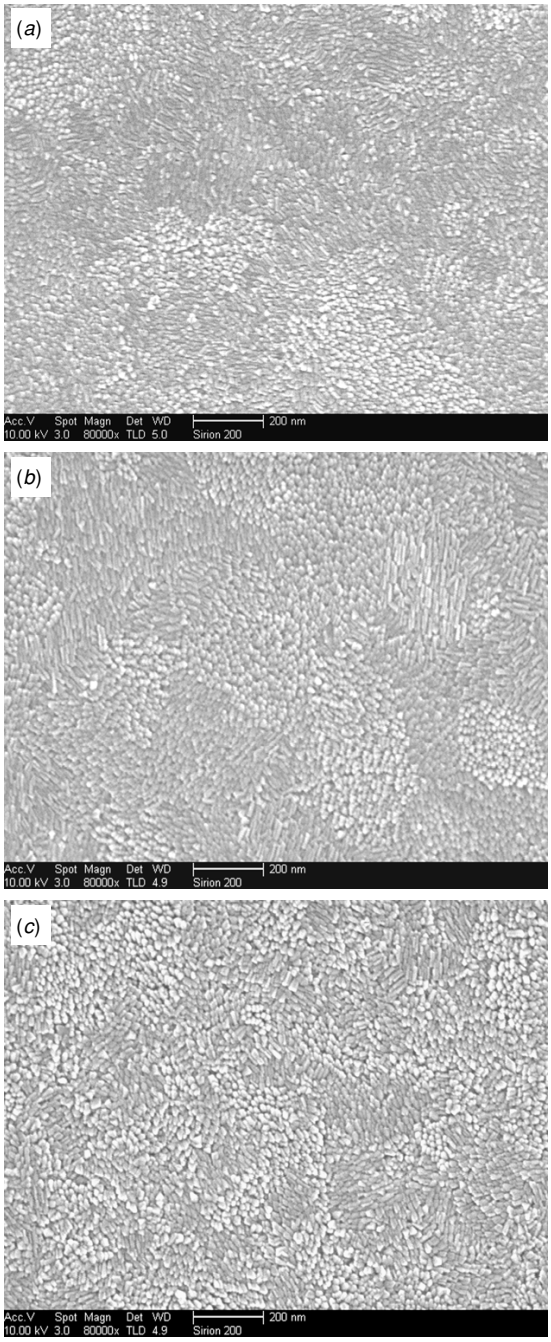

Figure 2. FESEM images of the TiO_2 thin films with O_2/Ar ratios of (*a*) 1:24, (*b*) 1:9 and (*c*) 2:1.

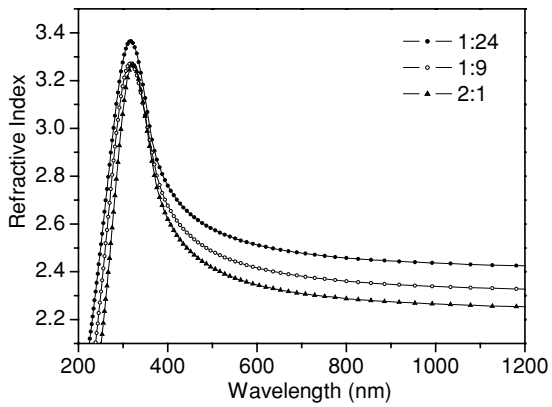

Figure 3. Spectral dependences of the refractive index for the TiO_2 thin films.

distribution too. This paper reports the analysis of the $|\sin\delta|$, ϕ and I_0 images and their selected area histogram and line plots to follow the structural and morphological change with oxygen stoichiometric condition variation in the deposited TiO_2 thin films.

3. Results and discussion

XRD traces and Raman spectra of the deposited TiO_2 films with those oxygen ratios are shown in figures 1(*a*) and (*b*). Both the XRD peaks (JCPDS 84-1286) and the Raman peaks (143.5, 393.8 and 634.9 cm^{-1}) confirm that the basic crystallographic structure of the TiO_2 film is anatase.

The FESEM images of those films (figure 2) show that the TiO_2 thin films consist of rod-like grains and have dimensions of about 40 × 10 nm, 58 × 12 nm and 52 × 18 nm for samples A, B and C, respectively. These grains have been found growing compactly either parallel or perpendicular to the film surface. In some areas they aggregated into clusters. The size of the aggregation varies with the O_2/Ar ratio, and the average size of the grain in and out of the aggregations slightly increases with increasing O_2/Ar ratio.

Figure 3 shows the refractive indices of TiO_2 thin films. One can see that the refractive indices decrease with increasing O_2/Ar ratio. Similar results were found in many materials such as ZnO, Al_2O_3, SiO_2 and ZrO_2 [20, 21]. The thicknesses of TiO_2 thin films are about 53, 69 and 83 nm for A, B and C, respectively, obtained from ellipsometry measurements. This result indicates that there is almost only one layer of rod-like grains perpendicular to the film surface. The refractive index is closely related to the density of material, being higher at higher density. It is considered that the decreased density of the thin film is responsible for the decease in refractive index with increasing O_2/Ar ratio.

Because of the realignment of the grains, the change of the film surface and the average TiO_2 structures can contribute to optical anisotropic changes such as the variation of the effective birefringence and the related slow axis vibration orientation sensitively. The birefringence ($|\sin\delta|$) and orientation (ϕ) images measured by the MetriPol have given the best logical data to follow the above grain size and aggregation variations and trace out the structural reasons. As can be seen in figure 4, the size, shape and structural composition of certain congregated particles in those films studied with different O_2/Ar ratios (30 × 30 μm^2 image area) change from sample A to sample C. A structural variation trend of the aggregation of particles can be described as (1) sample A film has less particle aggregation, (2) sample B film has more aggregation and (3) sample C film has least aggregation.

Figure 5 shows the birefringence ($|\sin\delta|$) and orientation (ϕ) plots along the lines in figure 4. Both ϕ and $|\sin\delta|$ plots of sample C show optical isotropic characteristics: random vibration orientation, close to zero birefringence value ($|\sin\delta| = 0$). The plots for sample B along the line across a cluster of nanoparticles show that the orientation varies but not randomly, and birefringence values may be small but vary above zero; these are the characteristics of weak optical

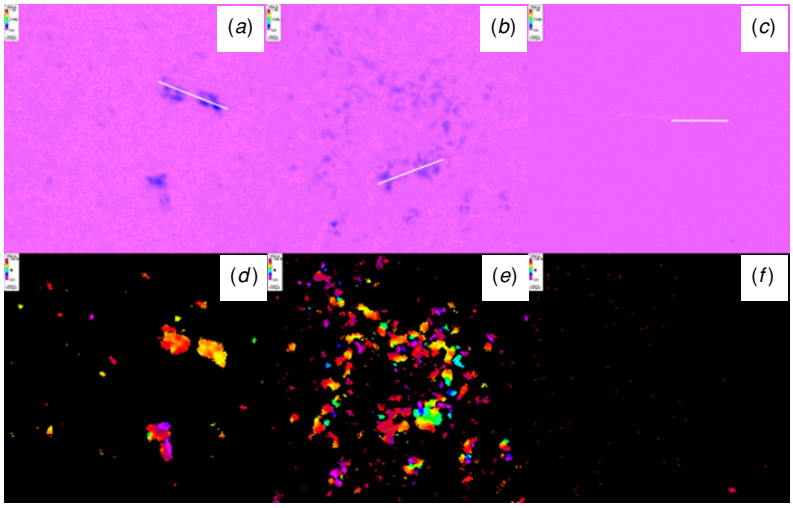

Figure 4. MetriPol $|\sin\delta|$ (*a*)–(*c*) and ϕ (*d*)–(*f*) images with 30 × 30 μm^2 image size for: (*a*) and (*d*) sample A (1:24); (*b*) and (*e*) sample B (1:9) and (*c*) and (*f*) sample C (2:1).

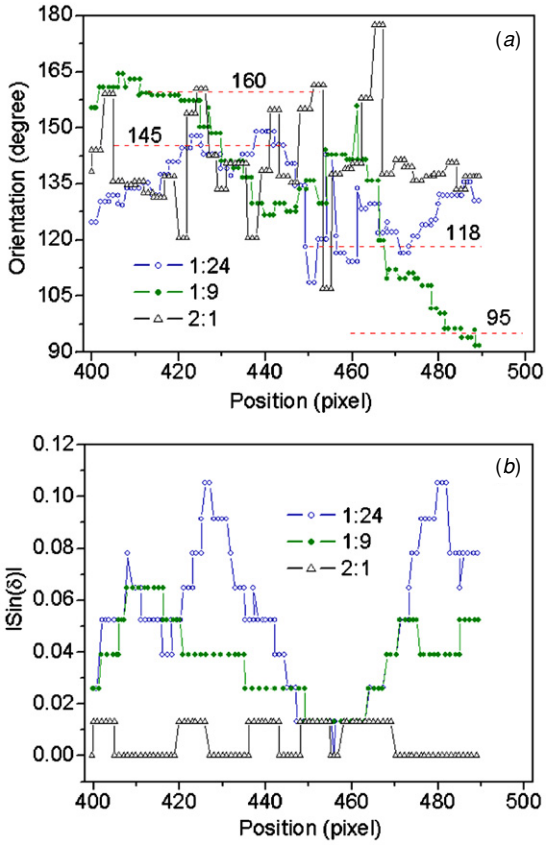

Figure 5. Orientation ϕ (*a*) and birefringence $|\sin\delta|$ (*b*) plots against pixel positions along a line on each image shown in figure 4.

anisotropy which is associated with more ordered structure character. A few easily recognizable orientation angles have been picked up and indicated by the drawing lines for sample B (figure 5(*a*)) which represent orientation variations across aggregated clusters (figures 4(*a*) and (*b*)). The cause of the orientation variation may be the structure or orientation change of aggregation particles. The same effect has been observed for sample A.

While the MetriPol zooms into areas about $18 \times 18\ \mu m^2$ in size with the minimum aggregation or visible clusters, in addition to the above general structural variation trends, a different sort of structural variation might also have been uncovered. It can be seen in figure 6 that some small aggregated clusters with excessively low birefringence have actually lowered the average optical anisotropy and so they have reduced the readable effective birefringence. Because they produce almost no optical anisotropy, they are seen as light pink dots in the $|\sin\delta|$ images and show no dot other than overall black in the ϕ images. In contrast, some of the other clusters have a slightly higher optical anisotropy and so the readable effective birefringence, which are indicated by the slightly darkening pink dots in the $|\sin\delta|$ and the non-black dots in the ϕ images. These results clearly suggest that rod-like TiO_2 grains in aggregated particles have two possible alignment orientations: parallel or perpendicular to the film or substrate surfaces (figure 2). In association with these two grain orientations there are two possible optical anisotropic readings: one with slightly high and the other with slightly low birefringence readings. When those rod-like grains are not clustered, as can be seen in the $|\sin\delta|$ image of the oxygen richest sample C (figure 6(*c*), they can be aligned randomly and have very low structure order so that the film dominated by this type of grain has very low birefringence readings. However, if they are crowded in an aggregated cluster they are found aligned in the above-described two possible orientations. In the case of the orientation perpendicular to the film surface, they are aligned with the microscopic optical axis so no or very low birefringence can be read, or, if they are orientated parallel to the surface, they are in the microscopic focal plane and alter the polarization states related transmissions to produce higher birefringence readings. The above-described colour and tone variations indicate the existence of both types (of rod-like grain orientation) of particle clusters in

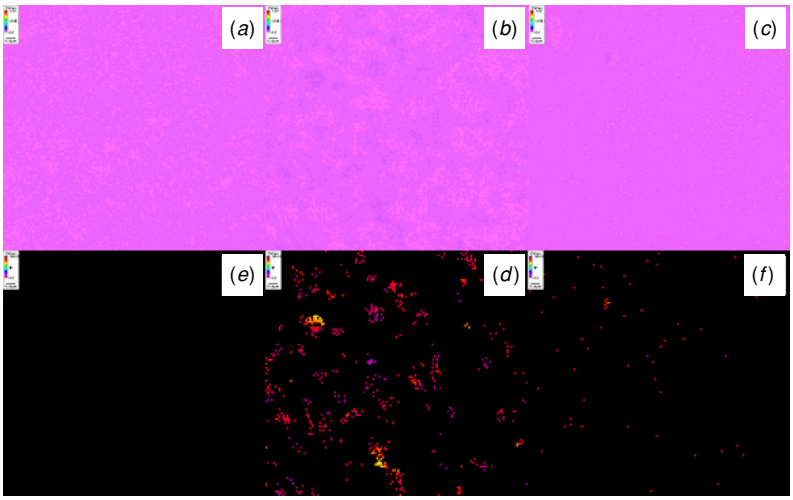

Figure 6. MetriPol $|\sin\delta|$ (*a*)–(*c*) and ϕ (*d*)–(*f*) images with $18 \times 18\ \mu m^2$ image size for: (*a*) and (*d*) sample A (1:24); (*b*) and (*e*) sample B (1:9) and (*c*) and (*f*) sample C (2:1).

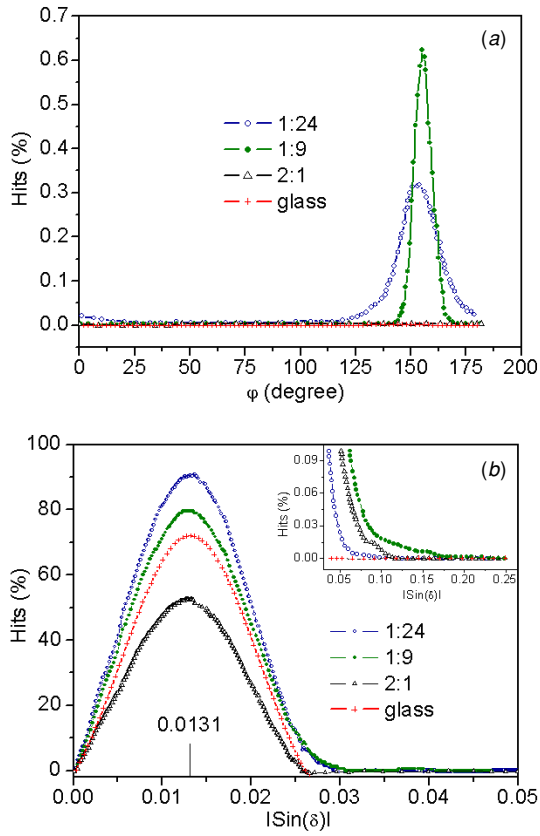

Figure 7. Histogram peaks of (*a*) ϕ and (*b*) $|\sin\delta|$ over all the pixels in figure 6.

the medium oxygen content sample B (figures 6(*b*) and (*e*)) and of mostly grain perpendicularly orientated clusters in the lowest oxygen content sample A (figures 6(*a*) and (*d*)). Figure 7 shows the plots of the histogram peaks of ϕ and $|\sin\delta|$ over all the pixels in the birefringence ($|\sin\delta|$) and orientation (ϕ) images in figure 6. These plots demonstrate that for the highest oxygen-containing sample C the vibration orientation is random and birefringence value is very low, further confirming the discovery of an optical isotropic characteristic of the film. While for the other two films, the vibration orientation varies but not randomly and birefringence values are relatively high and changeable, which further indicates the existence of different extents of optical anisotropy.

It is the authors' belief that the images and data results presented above have made good coincidence between the measurement of FESEM and birefringence images in the description of the optical characteristics of the TiO_2 thin films. The ratio of O_2/Ar during the sputtering of the films, which determines the oxygen content, can determine both the formation of aggregated rod-like grain clusters and the orientation of the grains in those clusters. It may be equally acceptable that the quantity of the aggregated clusters and the homogeneity of TiO_2 thin films change with the oxygen stoichiometric conditions as confirmed by the combination of refractive index and MetriPol measurement results.

4. Conclusion

MetriPol optical anisotropic imaging is an effective technique to study the morphological and optical characteristics of TiO_2 thin films. A clear trend of aggregation and rod-like TiO_2 grain orientation variations with the oxygen stoichiometric conditions has been observed in the sputtering deposited TiO_2 films. Both samples A and B have the tendency to form aggregated clusters within which the rod-like grains may orient differently. Sample C with the richest oxygen has been found to have the least tendency to aggregation so it has the highest structural and optical homogeneity. The MetriPol orientation and birefringence data and images have identified the parallel-to-film surface orientation of the rod-like grains in aggregated clusters as has been imaged by FESEM in sample B, so that with the medium oxygen content these types of orientations are orthogonal to those perpendicular to the film surface, which are found mostly in aggregated clusters in sample A containing the least oxygen.

Acknowledgment

This work was supported by Royal Society China/UK Joint Project (NC/China JP/15280).

References

[1] Yu J G 2004 *Rare Met.* **23** 289
[2] Kemmitt T, Al-Salim N I, Waterland M, Kennedy V J and Markwitz A 2004 *Curr. Appl. Phys.* **4** 189
[3] Sene J J, Zeltner W A and Anderson M A 2003 *J. Phys. Chem.* B **107** 1597
[4] Richards B S 2004 *Prog. Photovolt.* **12** 253
[5] Kumagai H, Toyoda K, Kobayashi K, Obara M and Iimura Y 1997 *Appl. Phys. Lett.* **70** 2338
[6] Nakayama T, Onisawa K, Fuyama M and Hanazono M 1992 *J. Electrochem. Soc.* **139** 1204
[7] Weinberger B R and Garber R B 1995 *Appl. Phys. Lett.* **66** 2409
[8] Lee C C, Chen H C and Jaing C C 2005 *Appl. Opt.* **44** 2996
[9] Busani T and Devine R A B 2005 *Semicond. Sci. Technol.* **20** 870
[10] Tang H, Prasad K, Sanjines R, Schmid P E and Levy F 1994 *J. Appl. Phys.* **75** 2042
[11] Chaure N B, Ray A K and Capan R 2005 *Semicond. Sci. Technol.* **20** 788
[12] Amor S B, Guedri L, Baud G, Jacquet M and Ghedira M 2003 *Mater. Chem. Phys.* **77** 903
[13] Wang Y L, Souche D, Zhang K Y, Fisson S, Vuye G and Rivory J 2000 *Thin Solid Films* **359** 171
[14] Li G H, Yang L, Jin Y X and Zhang L D 2000 *Thin Solid Films* **368** 164
[15] Anpo M, Dohshi S, Kitano M, Hu Y, Takeuchi M and Matsuoka M 2005 *Ann. Rev. Mater. Res.* **35** 1
[16] Karunagaran B, Kim K, Mangalaraj D, Yi J S and Velumani S 2005 *Sol. Energy Mater. Sol. Cells* **88** 199
[17] Moret M P, Zallena R, Vijay D P and Desu S B 2000 *Thin Solid Films* **366** 8
[18] Zekria D, Shuvaeva V A and Glazer A M 2005 *J. Phys.: Condens. Matter* **17** 1593
[19] Geday M A and Glazer A M 2004 *J. Phys.: Condens. Matter* **16** 3303
[20] Bachari E M, Ben Amor S, Baud G and Jacquet M 2001 *Mater. Sci. Eng.* B **79** 165
[21] Lee C C, Weu D T, Hsu J C and Shen C H 1996 *Thin Solid Films* **290–1** 88